Monthly Notices
of the
ROYAL ASTRONOMICAL SOCIETY

MNRAS **431,** 3364–3372 (2013)
Advance Access publication 2013 April 9

doi:10.1093/mnras/stt414

The complex nature of the nuclear star cluster in FCC 277⋆

Mariya Lyubenova,[1]† Remco C. E van den Bosch,[1] Patrick Côté,[2] Harald Kuntschner,[3] Glenn van de Ven,[1] Laura Ferrarese,[2] Andrés Jordán,[4,5] Leopoldo Infante[4] and Eric W. Peng[6]

[1]*Max Planck Institute for Astronomy, Königstuhl 17, D-69117 Heidelberg, Germany*
[2]*National Research Council of Canada, Victoria, BC V9E 2E7, Canada*
[3]*ESO, Karl-Schwarzschild-Str. 2, D-85748 Garching bei München, Germany*
[4]*Departamento de Astronomía y Astrofísica, Pontificia Universidad Católica de Chile, Av. Vicuña Mackenna 4860, Macul 7820436, Santiago, Chile*
[5]*The Milky Way Millennium Nucleus, Av. Vicuña Mackenna 4860, 7820436 Macul, Santiago, Chile*
[6]*Department of Astronomy, Institute for Astronomy and Astrophysics, Peking University, 5 Yiheyuan Road, Haidian, Beijing 100871, China*

Accepted 2013 March 5. Received 2013 February 11; in original form 2012 November 27

ABSTRACT

Recent observations have shown that compact nuclear star clusters (NSCs) are present in up to 80 per cent of galaxies. However, detailed studies of their dynamical and chemical properties are confined mainly to spiral galaxy hosts, where they are more easily observed. In this paper, we present our study of the NSC in FCC 277, a nucleated elliptical galaxy in the Fornax cluster. We use a combination of adaptive optics assisted near-infrared integral field spectroscopy, *Hubble Space Telescope* imaging and literature long-slit data. We show that while the NSC does not appear to rotate within our detection limit of ∼6 kms^{-1}, rotation is detected at larger radii, where the isophotes appear to be discy, suggesting the presence of a nuclear disc. We also observe a distinct central velocity dispersion drop that is indicative of a dynamically cold rotating sub-system. Following the results of orbit-based dynamical modelling, corotating as well as counter-rotating stellar orbits are simultaneously needed to reproduce the observed kinematics. We find evidence for varying stellar populations, with the NSC and nuclear disc hosting younger and more metal rich stars than the main body of the galaxy. We argue that gas dissipation and some level of merging have likely played an important role in the formation of the nucleus of this intermediate-mass galaxy. This is in contrast to NSCs in low-mass early-type galaxies, which may have been formed primarily through the infall of star clusters.

Key words: galaxies: elliptical and lenticular, cD – galaxies: formation – galaxies: kinematics and dynamics – galaxies: nuclei.

1 INTRODUCTION

It is now believed that up to 80 per cent of all galaxies host nuclear star clusters (NSCs) in their centres (e.g. Carollo, Stiavelli & Mack 1998; Böker et al. 2002; Côté et al. 2006). Typically, low- and intermediate-luminosity galaxies show a central light excess inside a characteristic radius $r_b \sim 0.02\, R_{\rm eff}$ above the inner extrapolation of the global light profile (Côté et al. 2007). These NSCs usually reside in the photometric centre of the galaxy (Binggeli, Barazza & Jerjen 2000; Böker et al. 2002) and their location overlaps with the kinematic centre (Neumayer et al. 2011). NSCs are usually brighter than typical globular clusters, compact ($r \sim 5$ pc), massive ($M \sim 10^7\, {\rm M}_\odot$), may be flattened, and often contain multiple stellar populations and complex structures (e.g. Walcher et al. 2005, 2006; Côté et al. 2006; Rossa et al. 2006; Seth et al. 2006, 2008; Barth et al. 2009; Piqueras López et al. 2012; Turner et al. 2012). Their masses seem to correlate with the mass of the host galaxies (Ferrarese et al. 2006; Wehner & Harris 2006), extending the super-massive black holes scaling relations to the low-mass end of galaxies. In some cases, NSCs appear to co-exist with central black holes (e.g. review by Graham & Spitler 2009, and references therein) and recently Neumayer & Walcher (2012) suggested that NSCs may be the precursors of massive black holes in galaxy nuclei. However, only handful of detailed studies on the properties of NSCs exists and these are mainly focused on such objects in late-type galaxies. Characterizing NSCs in early-type galaxies is a non-trivial task, both

⋆ Based on the observation collected at the ESO Paranal La Silla Observatory, Chile, Programme ID 380.B-0530, PI L. Infante

† E-mail: lyubenova@mpia.de

because of the high surface brightness of the underlying galaxy, and because of the NSCs compact sizes.

With the availability of adaptive optics (AO) fed integral field unit (IFU) instruments, this task is now becoming feasible. For example, Seth et al. (2010) have shown that the nucleus of NGC 404, a nearby S0 galaxy, hosts several morphologically and dynamically distinct components. The NSC in this galaxy shows a modest rotation aligned with the galaxy, a gas disc that rotates perpendicularly to the stars, and probably an intermediate-mass black hole ($\sim 10^5\,M_\odot$). Such complicated structure inevitably poses the question of how NSCs have formed. Currently, there are two main scenarios proposed. The first involves the dissipationless infall of star clusters to the galaxy centre due to dynamical friction (Tremaine, Ostriker & Spitzer 1975). The second suggests NSCs to be the result of dissipational sinking of gas to the galactic centre (Mihos & Hernquist 1994).

Numerical simulations of globular clusters infall have had certain success in reproducing the observed surface brightness profiles of nucleated galaxies, although with larger nuclei sizes comparing to what is observed (e.g. Oh & Lin 2000; Capuzzo-Dolcetta & Miocchi 2008a,b). However, more recently Hartmann et al. (2011) showed that star cluster accretion on to a pre-existing nuclear disc did not produce the observed line-of-sight kinematics of NSCs. They suggested that purely stellar dynamical mergers cannot be solely responsible for the formation of NSCs and that gas dissipation must also play a significant role in assembling the cluster's mass. What is the exact origin of this gas and how it gets transported to the galaxy nucleus is still under debate. Bekki, Couch & Shioya (2006) have shown that the dissipative merging of stellar and gaseous clumps formed from nuclear gaseous spiral arms in a gas disc eventually produce nuclei that rotate, are flattened and have a range of ages and metallicities. Pflamm-Altenburg & Kroupa (2009) concluded that compact star clusters with masses $\geq 10^6\,M_\odot$ act as cloud condensation nuclei and are able to accrete gas recurrently from a warm interstellar medium. This may cause further star formation events and account for multiple stellar populations in the most massive globular and NSCs. Recently, Turner et al. (2012) concluded that the dominant mechanism for nucleus growth in low-mass early-type galaxies is probably infall of star clusters through dynamical friction, while at higher masses, gas accretion resulting from mergers and torques becomes dominant.

In this paper, we present a detailed study of the nucleus in the intermediate-mass early-type galaxy FCC 277 (NGC 1428) and discuss our observations in the light of the current assumptions of nucleus formation. This galaxy is a member of the Fornax cluster and is part of the Advanced Camera for Surveys (ACS) Fornax Cluster Survey (Jordán et al. 2007). Its basic properties, as well as the main parameter of the natural guide star (NSC), are listed in Table 1. In Fig. 1, we show part of the *Hubble Space Telescope* (*HST*)/ACS z-band image, together with the field of view of Very Large Telescope (VLT)/SINFONI that we used to complete our study. In Fig. 2 *(left-hand panel),* we plotted the z-band surface brightness profile, together with the two Sérsic fits (dashed lines) that describe the galaxy light. The outer galaxy light is represented with a Sérsic fit with $n = 1.8$. The point where the nucleus starts to dominate over the inner extrapolation of the Sérsic fit is called break radius and for FCC 277 has the value $r_b = 0.25$ arcsec (indicated with an arrow in Fig. 2). The nucleus is fitted with another Sérsic profile with $n = 1.7$. For a detailed description of the fitting process see Turner et al. (2012); Ferrarese et al., in preparation.

The paper is organized as follows: in Section 2, we describe our observations and data reduction. In Section 3, we compare the

Table 1. Basic properties of FCC 277 and its Nuclear Star Cluster.

FCC 277		Reference
Morphological type	E5	Ferguson (1989)
B_T (mag)	13.8	Ferguson (1989)
Effective radius	10.2 arcsec	Ferguson (1989)
$(g-z)$ colour	1.31 ± 0.01	Blakeslee et al. (2009)
Distance	20.7 ± 0.7 Mpc	Blakeslee et al. (2009)
Major axis position angle	115°	Graham et al. (1998)
Velocity dispersion	$81.7\,\mathrm{km\,s^{-1}}$	Wegner et al. (2003)
$M^1_{\rm vir}$	$\sim 8 \times 10^9\,M_\odot$	
NSC		
Effective radius	0.09 arcsec$\sim$ 9 pc	Turner et al. (2012)
g (mag)	20.08 ± 0.16	Turner et al. (2012)
$(g-z)$	1.33 ± 0.18	Turner et al. (2012)

[1]Using $M_{\rm vir} = 5.0\,R_{\rm eff}\,\sigma^2/G$ (Cappellari et al. 2006).

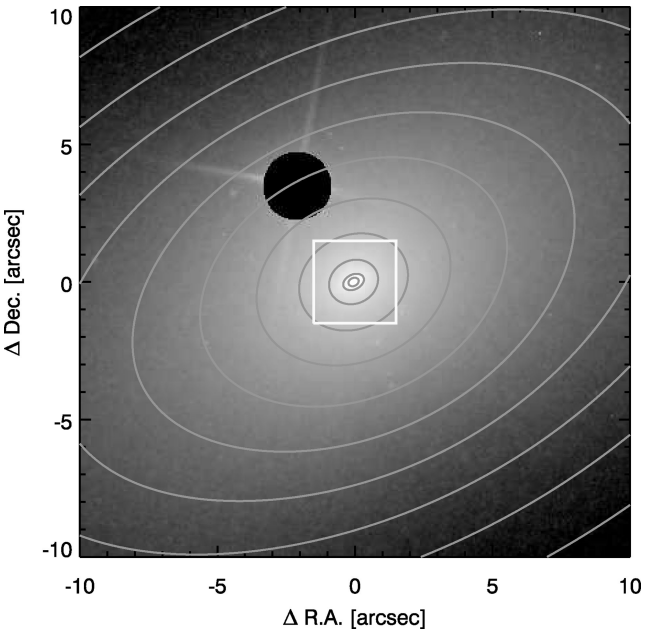

Figure 1. *HST*/ACS z-band image of FCC 277. The star that we used as an NGS for the AO correction is masked out here. The SINFONI field of view (3 arcsec × 3 arcsec) is indicated with a white box. The overlaid contours are from the MGE light model, discussed in Section 5.

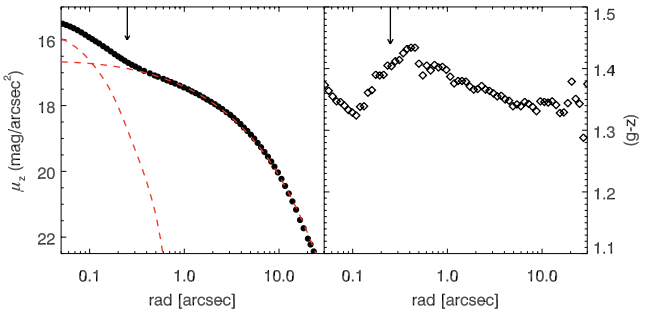

Figure 2. An *HST*/ACS z-band profile *(left-hand panel)* and $(g-z)$ colour *(right)* of FCC 277 (Turner et al. 2012; Ferrarese et al., in preparation). The coloured curves show the Sérsic fits to the two components: nucleus and galaxy. The arrows at 0.25 arcsec indicate the break radius, r_b, at which the nucleus component starts to dominate the galaxy light.

light profiles obtained from *HST*/ACS and VLT/SINFONI coupled with AO. Section 4 is devoted to the kinematics analysis of our IFU data, while in Section 5, we present results from dynamical modelling of the galaxy and the NSC. In Section 6, we explore the stellar populations of the nucleus of this galaxy. In Section 7, we discuss our findings in the light of current galaxy and NSC formation models. We conclude in Section 8.

2 OBSERVATIONS AND DATA REDUCTION

2.1 Observations

We obtained integral field spectroscopy of the Fornax E5 galaxy FCC 277 (NGC 1428) using VLT/SINFONI (Eisenhauer et al. 2003; Bonnet et al. 2004) in Natural Guide Star AO mode on 2007 October 6, 7 and 10 (programme ID 380.B-0530, PI L. Infante). We used the *K*-band grating (1.95–2.45 μm) that gives a spectral resolution $R\sim3500$ [6.2 Å full width at half-maximum (FWHM) as measured on sky lines]. Our observations cover the central 3 arcsec × 3 arcsec, with a spatial sampling of 0.05 arcsec × 0.10 arcsec . As a natural guide star we used an $R = 14$ mag star located at 3.5 arcsec to the north of the galaxy centre (see Fig. 1). Due to its proximity to the galaxy centre, this star does not appear in the guide star catalogue or the US Naval Observatory (USNO) catalogue as a separate entry. Its celestial coordinates are α(J2000) = 03:42:22.9 and δ(J2000) = −35:09:11.4. Our observations were carried out in service mode.

For the observations we used the standard near-infrared (IR) nodding technique. Each observing block consisted of a sequence of object and sky frames (OOSOOSOOS), each individual integration was 300 s, the sky fields were offset by 50 arcsec to the north. Science frames were dithered by 0.05 arcsec and 0.15 arcsec in order to reject bad pixels. There were six observing blocks. The total on-source integration time was 3 h. Additionally, after each observing block and at a similar airmass, we observed a *B* dwarf to act as a telluric star.

2.2 Data reduction

We used the ESO SINFONI pipeline v2.0.5 to perform the basic data reduction on each observing block, consisting of six object and three sky exposures. In brief, the pipeline extracts the raw data, applies distortion, bad pixels and flat-field corrections, wavelength calibration, and stores the combined sky-subtracted spectra from one observing block in a 3D data cube. For each resulting data cube, we then ran the LAC3D code (Davies et al. 2010) to detect and correct residual bad pixels identified using a 3D Laplacian edge detection method.

We reduced the telluric stars in the same way as the science frames. Then for each telluric star we extracted a one-dimensional spectrum, removed the hydrogen Brackett γ absorption line at 2.166 μm after fitting it with a Lorentzian profile, and divided the star spectrum by a blackbody spectrum with the same temperature as the star. The last step in preparing the telluric spectrum was to apply small shifts (<0.05 pixels) and scalings to minimize the residuals of the telluric features. To do this, we extracted a central one-dimensional spectrum from each science data cube and cross-correlated and fitted it with the corresponding telluric spectrum. Then we divided each individual spaxel in the six galaxy data cubes by the corresponding best-fitting telluric spectrum. In this way we also obtained a relative flux calibration.

Finally, we combined the six galaxy data cubes, using a 3σ-clipping pixel reject algorithm. We also reconstructed a two-dimensional image of the galaxy, after integrating the spectral dimension of the final data cube in the range 2.1–2.4 μm, where the contamination from sky lines residuals is minimal. To be able to robustly measure the velocity and velocity dispersion from the spectra of the galaxy a minimum S/N of 20 per pixel is required. Because the SINFONI pipeline does not provide error propagation during data reduction, we estimated the noise in each spectrum of the data cube as the rms of the residuals after subtracting a smoothed model of the spectrum. Then, we used this noise estimate to bin the final galaxy data cube to achieve an approximately constant S/N ∼ 25 using the Voronoi 2D binning method of Cappellari & Copin (2003). This S/N allowed us to conserve a good spatial resolution (our smallest bins in the centre are ∼0.1 arcsec across), while we are still able to reliably extract the stellar kinematics.

3 COMPARISON BETWEEN VLT/SINFONI AND *HST*/ACS LIGHT PROFILES

In Fig. 3, we compare the light profiles of FCC 277 derived from *HST*/ACS imaging and VLT/SINFONI observations. This galaxy is part of the ACS Fornax Cluster Survey (Jordán et al. 2007) and high spatial resolution imaging in the *g* band and *z* band from the ACS is available. We used the IRAF task *ellipse* to fit elliptical isophotes to the ACS *z*-band image (black symbols in Fig. 3) and to the SINFONI reconstructed image (before binning; red symbols). In panel (a) the two luminosity profiles are compared, after being normalized in the region 0.5 arcsec – 0.7 arcsec (dashed vertical lines). Isophotal parameters are plotted against the semimajor axis length. The vertical arrows denote the break radius, $r_b = 0.25$ arcsec, at which point the nuclear component starts to dominate the surface brightness profile (Côté et al. 2007, see also Fig. 2).

Although observed with AO, the SINFONI light profile is less steep than the ACS profile within the inner ∼0.3 arcsec. Assuming this is due to the lower spatial resolution of the SINFONI data, we estimated their point spread function (PSF) to be 0.165 arcsec

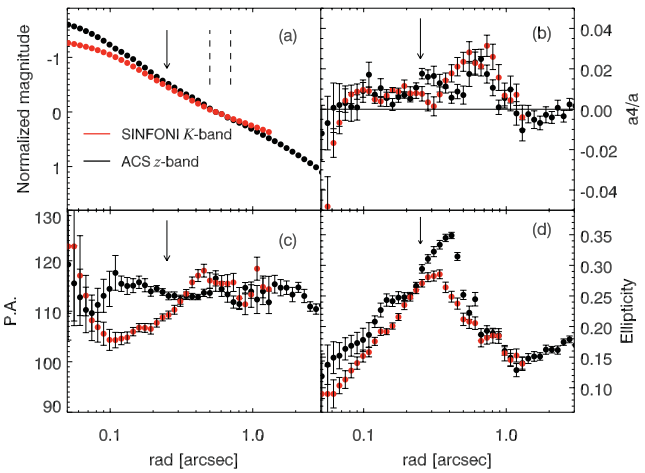

Figure 3. Comparison between isophotal parameters obtained from space and AO ground-based imaging. The red symbols show the light profile of FCC 277 as derived from our SINFONI *K*-band reconstructed image. The black symbols denote *HST*/*ACS* *z*-band imaging. The two vertical dashed lines in panel (a) show the area where the two profiles were normalized (0.5 arcsec $< r <$ 0.7 arcsec). The vertical arrows in each panel indicate the break radius, as in Fig. 2. In panel (b) we compare the fourth cosine term of the isophotal fits that is indicative for deviations from pure elliptical shape. In panel (c) the measured PAs are displayed, and in panel (d) the ellipticity of the isophotes is shown.

(FWHM) by convolving the ACS image (using a Tiny Tim PSF, Krist 1995) with a given Gaussian PSF until it matches the light distribution in the SINFONI image (observations of stellar PSFs were not obtained during the SINFONI run).

In panel (b) of Fig. 3, we plotted the cosine fourth-order Fourier coefficient of the isophotes, divided by the semimajor axis length. Positive values of this parameter are indicative of discy isophotes, as are observed in both the z- and K-band images in the inner 1 arcsec. There are two peaks in the $a4/a$ profile, one at ∼0.2 arcsec, coinciding with the break radius, and a stronger second peak at ∼0.6 arcsec, coinciding with the peak in the velocity field (see Section 4). In panel (c), no significant variations of the position angle (PA) outside of the break radius are observed and the mean PA is consistent with the one derived at larger radii (see Table 1). In panel (d), the ellipticity reaches a maximum at ∼0.35 arcsec for both the ACS and SINFONI profiles, although with different amplitudes. These differences are expected due to the differences in the PSF of the two images; a larger PSF leads to rounder isophotes (Peletier et al. 1990). The comparison of the two profiles led us to the conclusion that the SINFONI ground-based AO assisted observations are similar in quality to the *HST*/ACS images.

The observed features of the isophotal parameters point to a picture where, within the break radius, the NSC may be flattened or, alternatively, may be the superposition of a round NSC and a larger scale disc. Such nuclear disc beyond the break radius is evident in the disciness parameter $a4/a$ at ∼0.6 arcsec (see also Turner et al. 2012).

4 STELLAR KINEMATICS

We used the PPXF code (Cappellari & Emsellem 2004) to derive the first and second order of the line-of-sight velocity distribution, working with a library of seven template spectra of K and M giant stars. These templates were observed with the same instrument and the same setup as our science target. To find the best-fitting composite template spectrum, we used the region between 2.1 and 2.36 μm, where several strong absorption features allow accurate measurements (see Fig. 4), and masked the strong near-IR sky lines (Rousselot et al. 2000). In Fig. 4, we show the spectrum of a central bin in the galaxy with the overplotted best-fitting composite template as derived by the PPXF code (in red), as well as the residuals (in grey).

Our stellar mean velocity and velocity dispersion maps are shown in Fig. 5. Using kinemetry, described by Krajnović et al. (2006), we extracted the velocity and velocity dispersion profiles, shown with filled symbols in Fig. 6. We observe rotation around the

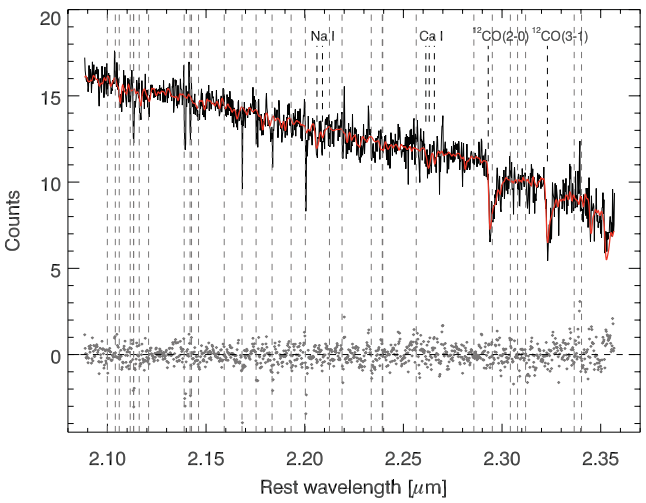

Figure 4. The spectrum from the central bin (S/N∼25) of FCC 277 with an overplotted best-fitting template spectrum, derived by the PPXF code (red line; fit residuals are shown in grey). The location of the strongest near-IR absorption features in the K band is indicated. The dashed vertical lines show the location of the strongest sky emission lines.

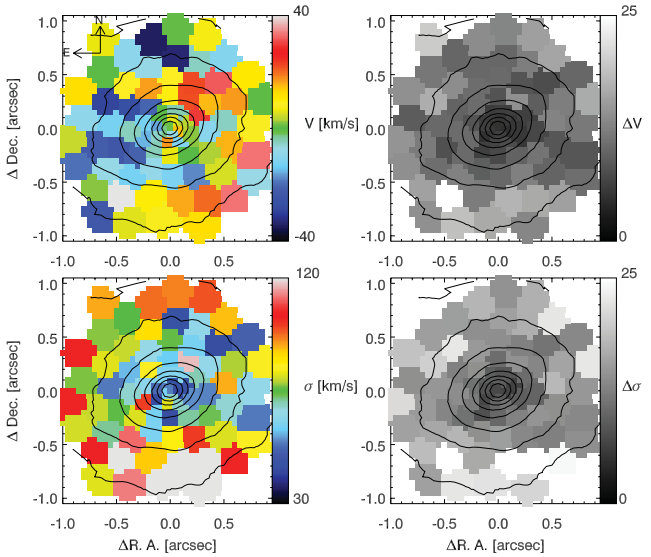

Figure 5. Velocity (*top panel*) and velocity dispersion (*bottom panel*) maps of FCC 277 and corresponding errors *(right-hand panels)*. Overplotted are contours with constant surface brightness, as derived from our reconstructed SINFONI K-band image.

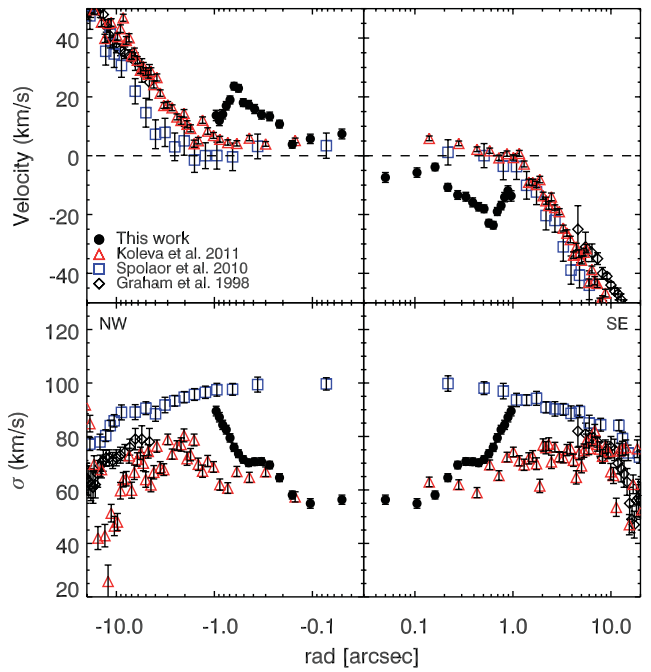

Figure 6. Behaviour of the stellar kinematics at different spatial scales. Long-slit kinematics data from Graham et al. (1998, diamond symbols), Spolaor et al. (2010, blue squares) and Koleva et al. (2011, red triangles) are shown. With solid symbols we plotted the innermost kinematics profile of FCC 277, extracted from the SINFONI maps using kinemetry.

minor axis of the galaxy up to $\pm 25\,\mathrm{km\,s^{-1}}$ at $r \sim 0.6$ arcsec, which is outside the break radius of the luminosity profile (r_b=0.25 arcsec, see Fig. 2, left-hand panel) where the NSC is supposed to reside. At the centre of the galaxy, the velocity dispersion approaches $\sim 55\,\mathrm{km\,s^{-1}}$ and then it increases in the outer parts of the field of view to reach $\sim 90\,\mathrm{km\,s^{-1}}$ at $r \sim 1$ arcsec.

In Fig. 6, we also compare our own SINFONI data with a compilation of literature measurements, derived using long slits, aligned along the major axis of the galaxy. Graham et al. (1998, diamond symbols) used a spectrograph with a slit width 2 arcsec on the Australian National University's 2.3 m telescope at Siding Spring Observatory. Their data do not cover the inner 4 arcsec of the galaxy, due to the presence of a relatively bright star close to the nucleus (that we used as a natural guide star for the AO). Spolaor et al. (2010, blue squares) used the GEMINI/Gemini Multi-Object Spectrograph (GMOS) instrument with a slit width of 1 arcsec. The seeing during these observations was in the range 0.7–1 arcsec. Koleva et al. (2011, red triangles) re-analysed the same observations.

Based on Fig. 6, we conclude that the rotating sub-structure in the nucleus of FCC 277 corotates with the main body of the galaxy and that the velocity dispersion in the outer regions of the SINFONI field of view reaches similar values as the long-slit studies. We note that the spatial resolution of our AO supported data is much higher than the resolution achieved by the other three studies, thus we cannot directly compare the radial profiles at small galactocentric radii. The significantly worse spatial resolution of the long-slit observations means that the inner rotation and velocity dispersion dip are washed out.

The observed rotation, taken together with the drop in the velocity dispersion, indicates the presence of a corotating cold sub-structure in the inner 0.6 arcsec of the galaxy. We fitted the kinematic PA of this sub-structure using the method described in appendix C of Krajnović et al. (2006). The measured value is $118^\circ \pm 10^\circ$, which is consistent with the photometric PA of the main body of the galaxy, derived at larger radii (see Table 1).

For early-type galaxies the apparent stellar angular momentum λ_{R_e} and the galaxy flattening are now a commonly used tool to classify galaxies into *fast* and *slow* rotators (Cappellari et al. 2007; Emsellem et al. 2007). The method needs IFU data to measure λ_{R_e} inside one-effective radius. For FCC 277 only long-slit data are available out to the effective radius. Thus, we used our best-fit Schwarzschild model from Section 5 to simulate the velocity and velocity dispersion as they would be observed by an IFU. We measured $\lambda_{R_e} = 0.3$. Using the most recent classification from Emsellem et al. (2011), we found that this galaxy is a *fast* rotator and lies slightly above the dividing line between the two classes, with its ellipticity $\epsilon = 0.3$.

5 DYNAMICAL MODELLING

To measure the mass distribution and the orbit configuration of the inner part of FCC 277, we used Schwarzschild (1979) modelling. This method (van den Bosch et al. 2008) works by constructing a trial mass model of the galaxy, including a black hole, stars and dark halo. Then, the gravitational potential is inferred from the mass model and representative orbits are integrated numerically, while keeping track of the paths and orbital velocities of each orbit. We can then create a mass model of the galaxy by assigning an amount of mass to each orbit so that the overall stellar mass distribution is reproduced, while simultaneously fitting the observed stellar kinematics. The effect of the PSF on the observed stellar kinematics is an integral part of the dynamical model. These models have the advantage that they do not require any assumptions regarding the orbital anisotropy of the galaxy.

The models were constructed as follows. First, we parametrized the galaxy stellar surface brightness using the multiGaussian expansion (MGE) method, described by Cappellari (2002), on the ACS z-band image. In Fig. 1, we show this image with overlaid contours of the MGE light model. There were 13 Gaussians with varying flattening fitted in total, the first two of them describing the NSC. The galaxy shows strong rotation around the minor axis and we therefore assumed the galaxy is oblate axisymmetric, which is the most common configuration (e.g. Padilla & Strauss 2008). The galaxy is also strongly flattened, with a minimum flattening 0.6 at 15 arcsec, and can thus not be seen more face-on than $i = 65^\circ$. Then we used our symmetrized (using the method described in appendix A of van den Bosch & de Zeeuw 2010) SINFONI IFU kinematics from Section 4 and the Schwarzschild orbit superposition method (van den Bosch et al. 2008) to construct a realistic dynamical model for the galaxy and the NSC. We also included the long-slit data of Graham et al. (1998), to be able to constrain the mass-to-light ratio (M/L) of the main body of the galaxy. We did not include the data of Spolaor et al. (2010) and Koleva et al. (2011), which result from two different reductions of the same data set, because they do not match with our kinematics measurements for the inner parts of the galaxy. We probed the following parameters: the central black hole mass and separate M/L for the galaxy and the NSC, using 5000 dynamical models. Changes in the inclination between 65° and 90° led to insignificant changes in the M/L, thus we marginalized over it.

In Fig. 7, we show the input symmetrized SINFONI kinematics velocity and velocity dispersion maps *(left-hand panels)* together with the resulting kinematics obtained by the best-fitting dynamical model *(middle panels)*. The reduced χ^2 of the best models is ~ 0.21 over the 81 SINFONI bins. The low value of the reduced χ^2 is due to the very conservative estimate of our kinematics errors. The best-fitting $\mathrm{M/L_z}$ of the galaxy and NSC is 3.2 ± 0.4 and 3.0 ± 1.0, respectively, as shown in Fig. 8. Confidence intervals are determined using $\Delta\chi^2$ statistics, assuming two degrees of freedom. Thus, the mass of the NSC is $1.4 \pm 0.4 \times 10^7\,\mathrm{M_\odot}$. The black hole mass is unconstrained, as the uncertainties on the central kinematics are too large. The difference in velocity dispersion between a 10^5 and a $10^7\,\mathrm{M_\odot}$ black hole is 5 $\mathrm{km\,s^{-1}}$ and the uncertainties on σ are $\sim 15\,\mathrm{km\,s^{-1}}$. Black hole masses above $10^7\,\mathrm{M_\odot}$ do yield significantly worse fits and hence we place an upper limit of $10^7\,\mathrm{M_\odot}$. To robustly determine the black hole mass, higher S/N spectra of the nucleus need to be obtained to reduce the uncertainties on the central kinematics and the PSF of the IFU data needs to be known precisely. The inclusion of a dark matter halo does not alter the M/L of the NSC and only very weakly the M/L of the galaxy. The $\mathrm{M/L_{gal}}$ is expected to contain only a small contribution from the dark matter (Cappellari et al. 2006), hence our final adopted model does not include a dark matter halo. Kinematics reaching much further out are needed to properly constrain the dark matter halo.

Apart from the mass distribution of the galaxy, the models yield the orbital distribution as a function of radius. In Fig. 9, we show the orbital mass weights as a function of the average radius and spin $\bar{\lambda}_z = \bar{J}_z \times (\bar{r}/\bar{\sigma})$, where $\bar{J}_z$ is the average angular momentum along the short z-axis and $\bar{\sigma}$ the average second moment of the orbits.

We detect the presence of three distinct components: both a corotation and counter-rotating component as well as a non-rotating bulge component. The relative contribution of each of these components is shown in the *bottom panel* of Fig. 9. Both rotating

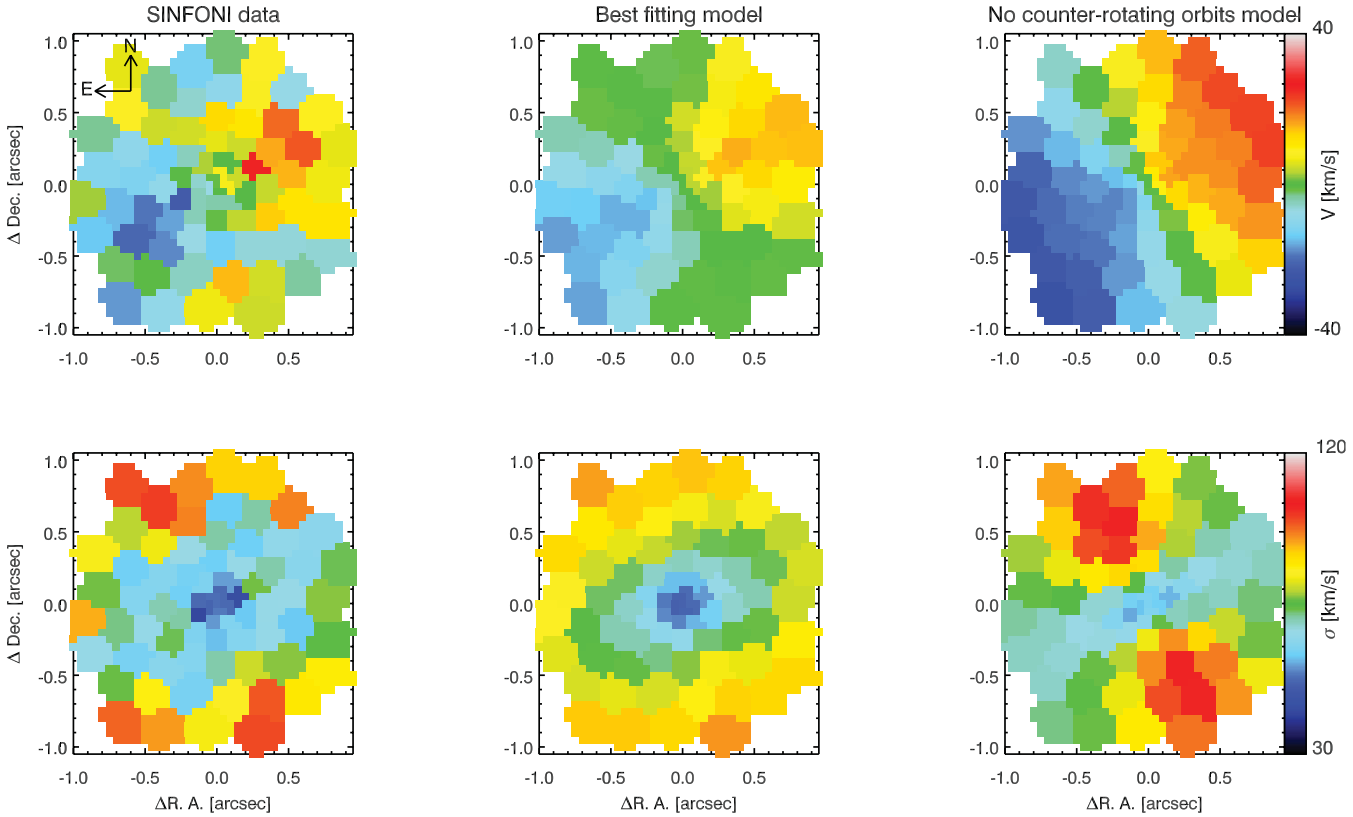

Figure 7. Comparison between our symmetrized SINFONI kinematics *(left-hand panels)* and the ones obtained by the best-fitting dynamical model *(middle panels)*. The *right-hand panels* show the resultant kinematics maps from our best-fitting model when we do not include stars on counter-rotating orbits.

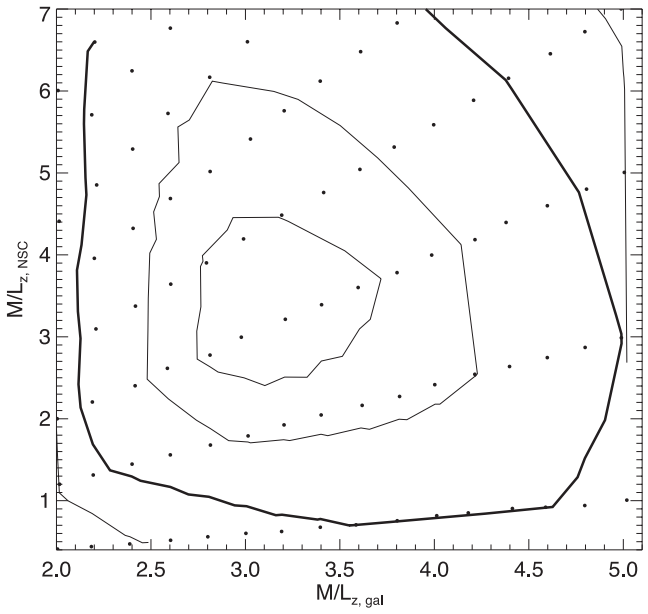

Figure 8. Confidence interval of the dynamical models of FCC 277 for the M/L in z-band. The black dots indicate the location of the models and the contours indicate 1, 2 and 3σ intervals, where the 3σ level is indicated by a thick line.

components extend well inside the break radius and have similar contributions in the NSC region. The sigma drop seen in the stellar dispersion map coincides with a decrease of the non-rotating orbits. The question arises if this is the only possible orbital configuration

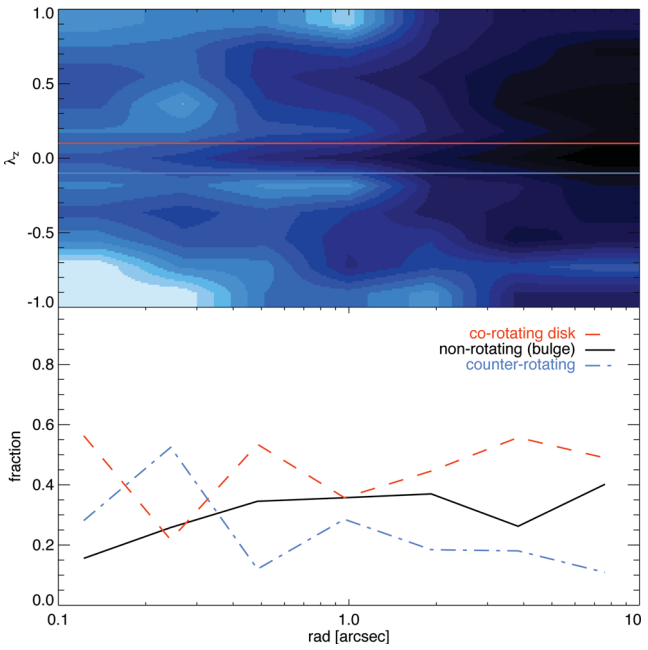

Figure 9. Top panel: distribution of mass along the orbits of our best-fitting dynamical model, as a function of angular momentum and radius. The colour coding reflects a factor of 3.5 span in mass density (darker colour corresponds to higher mass). Bottom panel: fraction of non-/rotating orbits as a function of radius. A non-rotating bulge ($-0.1 < \lambda_z < 0.1$) is denoted with a black line. The red line corresponds to the sum of all corotating orbits with $\lambda_z > 0.1$, the blue line – all counter-rotating orbits with $\lambda_z < -0.1$.

for this system. The orbits available to the Schwarzschild models are a fully representative set and the linear solver used to construct the models is guaranteed to find the global minimum (van de Ven, de Zeeuw & van den Bosch 2008; van den Bosch et al. 2008). This guarantees that the model finds the best-fitting orbital configuration. There could be other solutions that are also a good representation of the observations. As a consistency check, we attempted to fit models without counter-rotating orbits, which would exclude an opposite angular momentum accretion event as a formation scenario for the nucleus. However, this led to a significantly worse match of the stellar kinematics (see Fig. 7, *right-hand panels*), which indicates that counter-rotating orbits are thus required.

We note that we were unable to use the Jeans' modelling approach to fit the stellar kinematics using the method described by Cappellari (2008). Although we could receive reasonable fits to the second velocity moment ($V_{\rm rms}$), the fits to the velocity field were unsatisfactory. This is because, as it is at the moment, the JAM package does not allow the rotation parameter κ to accept positive and negative values simultaneously for a given MGE Gaussian.

To be able to quantitatively discuss the different orbital fractions, the dark matter halo of the galaxy and its global M/L, one would need improved long-slit or other large-scale kinematics.

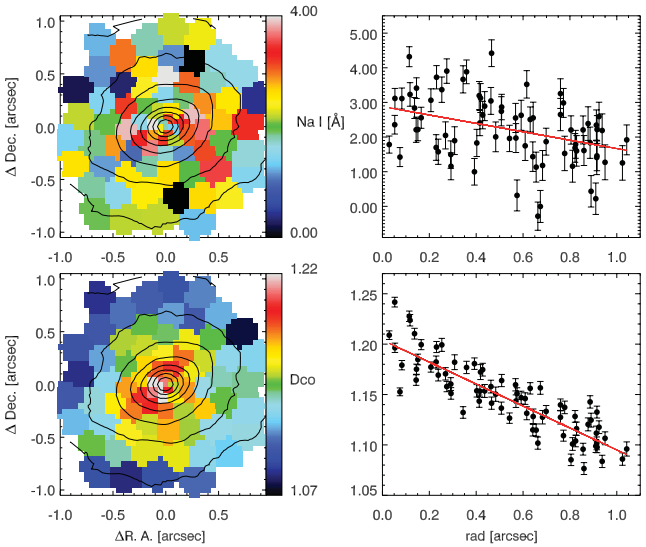

Figure 10. Na I and $D_{\rm CO}$ index maps with *HST* like spatial resolution *(left-hand panels)* and radial profiles *(right-hand panels)*. The red solid lines are the least-squares linear fits to the data.

6 STELLAR POPULATION PARAMETERS

In addition to the structure and dynamics, we can investigate what the parameters of the stellar populations of the NSC and/or nuclear disc in the heart of FCC 277 are and whether they differ from the main body of the galaxy.

Usually, nuclei in low-luminosity Fornax and Virgo galaxies are bluer compared to their hosts (Côté et al. 2006; Turner et al. 2012). In the right-hand panel of Fig. 2, we show the $(g-z)$ colour profile, as derived from *HST*/ACS imaging (Turner et al. 2012; Ferrarese et al., in preparation). The integrated colour of the nucleus is $(g-z) = 1.33 \pm 0.18$ (Turner et al. 2012) and does not differ from the main body of the galaxy. If nuclei follow the same colour–metallicity relation as globular clusters in early-type galaxies do (Peng et al. 2006), then the red colour would be indicative for higher metallicity of the NSC. However, age effects cannot be excluded, due to the well-known age–metallicity degeneracy of broad-band colours.

Koleva et al. (2011) measured from optical spectroscopy the age and metallicity of the core of FCC 277 (within a 0.5 arcsec radius aperture) to be 5.4 Gyr and [Fe/H] $= -0.07$, respectively. At the effective radius these values are 7.7 Gyr and [Fe/H] $= -0.50$. Their data lack the spatial resolution to differentiate the NSC and the disc; however, there is a pronounced negative age and positive metallicity gradient towards the nucleus.

We used our near-IR IFU spectra to measure the line strengths of Na I (∼2.2 μm) and ^{12}CO (2–0) (∼2.3 μm) absorption features (see Fig. 4). From previous stellar population studies in the near-IR wavelength range we know that the Na I index increases with metallicity and younger age (Silva, Kuntschner & Lyubenova 2008; Mármol-Queraltó et al. 2009; Lyubenova et al. 2010), and the $D_{\rm CO}$ index is expected to increase with higher metallicity for ages above 3 Gyr (Maraston 2005).

We measured the two indices using the definition of Frogel et al. (2001) for the Na I index and Mármol-Queraltó et al. (2008) for the $D_{\rm CO}$ index. Before measuring, we first broadened our spectra to 6.9 Å (FWHM, ∼ 94 kms^{-1}) to match the spectral resolution of other stellar population studies of elliptical galaxies in the near-IR (e.g. Silva et al. 2008; Mármol-Queraltó et al. 2009). Finally, we corrected the Na I index to zero velocity dispersions using the velocity dispersion corrections of Silva et al. (2008).

In Fig. 10, we show our index maps as well as their radial profiles. We observe radial gradients for both indices. Increase in Na I towards the centre is consistent with increasing metallicity and/or younger age in the nuclear disc and NSC. On the $D_{\rm CO}$ map, we see that the strongest index values towards the centre seem to form an elongated shape, aligned with the major axis of the galaxy and the rotating structure, visible on the velocity map (Fig. 5.) This increase is again consistent with the redder colour and indicative of higher metallicity.

In Fig. 11, we compare FCC 277 with other early-type galaxies in the Fornax cluster in terms of their Na I and $D_{\rm CO}$ indices versus their central velocity dispersion. The spectra of Silva et al. (2008) cover 1/8 of the effective radius of each galaxy and are marked with circles. Open circles represent galaxies with old stellar populations, solid symbols stand for the galaxies that have optical signatures of recent (<3 Gyr) star formation. The dashed line illustrates the least-squares linear fit to the old galaxies only. Our SINFONI observations of FCC 277 cover approximately the same radial extent as the other galaxies. We plotted the values measured on the integrated spectrum with solid blue squares. We extracted the NSC area ($r \leq 0.25$ arcsec) and marked our measurements with orange asterisks. With open red diamonds, we indicated the values for the so called 'nuclear disc', integrated over the range 0.25 arcsec $< r \leq 0.7$ arcsec.

The Na I index of the NSC is much higher compared to the extrapolation (shown with a dotted line) of the σ–Na I relation for old Fornax galaxies and is closer to the systems with younger (<3 Gyr) stellar populations. There is not a big difference of the index strength between the nuclear disc and the galaxy as a whole, so one would infer purely old age for these two components if looking only at this plot. The $D_{\rm CO}$ index seems to saturate for galaxies with velocity dispersion higher than 100 kms^{-1}. Until reliable stellar population models for the near-IR become available, we cannot provide a quantitative estimate for the changes in stellar population parameters in the nuclei of early-type galaxies. At the moment, we can only speculate that, taken together with the red colour of the NSC (as red as the host galaxy, which is unusual for NSCs in Fornax

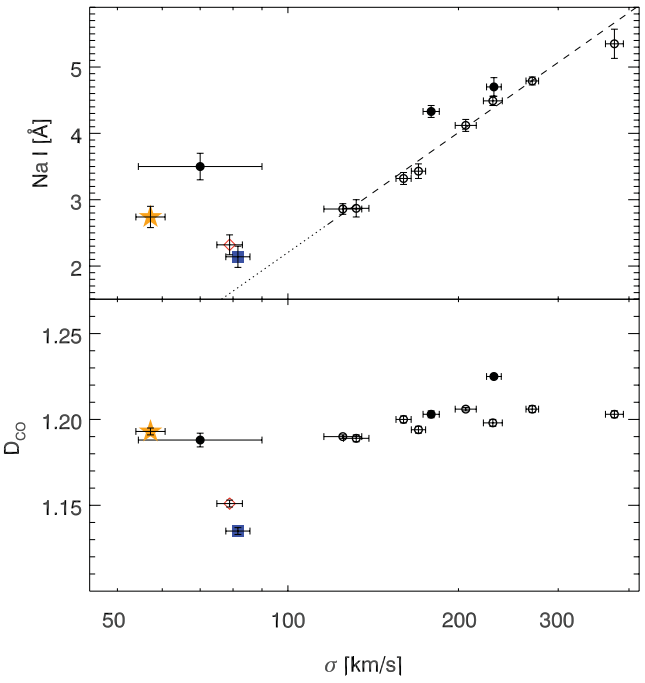

Figure 11. Na I and D_{CO} indices versus the central velocity dispersion of Fornax early-type galaxies. Open symbols denote old Fornax galaxies, solid symbols – galaxies with optical signatures of recent (<3 Gyr) star formation (Silva et al. 2008). The dashed line represents the least-squares linear fit to the old Fornax galaxies only, the dotted line denotes its extrapolation to lower σ. The NSC in FCC 277 is marked with an orange asterisk, the so called nuclear disc – with a red diamond, and the whole galaxy, as observed with SINFONI, is marked with a blue square.

as discussed above), these point to a mixture between younger age and higher metallicity compared to the main body of the galaxy.

7 FORMATION MECHANISM OF THE NSC

So far we have collected evidence that: (i) the NSC inside the central 0.25 arcsec of FCC 277 does not rotate within our error of ∼6 kms^{-1}; (ii) the rotation visible at ∼0.6 arcsec overlaps with a maximum in the disciness of the isophotes, suggesting the existence of a nuclear disc around the NSC; (iii) the existence of a central velocity dispersion drop is indicative of significant rotation in the same area; (iv) dynamical modelling reveals a significant rotation in the inner 1 arcsec in *both* directions, i.e. corotation and counter-rotation, explaining the low level of observed rotation, the low λ_{R_e} and the sigma drop; (v) there is no significant difference in the derived dynamical M/L between the NSC and the galaxy. However, within the errors, a change in the stellar population parameters may not lead to an obvious change in the M/L for the different components. The derived dynamical M/L_z within the errors is consistent with the predictions of stellar population models for a Salpeter initial mass function (IMF) and 5−10 Gyr age (e.g. Bruzual & Charlot 2003; Maraston 2005). If one compares to Chabrier or Kroupa IMF, then our dynamical M/L_z is about a factor of 2 larger ; (vi) there is evidence for differences in the stellar population parameters of the NSC, the nuclear disc, and the galaxy. This points to a scenario where the nucleus is younger and more metal rich.

All these pieces of evidence for complex kinematics and stellar populations point to a scenario where the NSC and disc formed through multiple episodes of gas accretion and subsequent episodes of star formation. Counter-rotation points towards mergers with orbital angular momentum opposite to the host galaxy. Seth et al. (2010) reached the same conclusion for the nucleus in NGC 404, a nearby S0 galaxy. Thus, FCC 277 is the second early-type galaxy that has an NSC exhibiting complex star formation history. Turner et al. (2012) noted that the lowest mass galaxies with nuclei in the ACS Fornax and Virgo Cluster Surveys seemed to be structurally simple, having likely formed through star cluster infall. The more massive galaxies (such as FCC 277) seemed to be more structurally complex in their inner regions. They interpreted that as evidence for an increased importance of gas infall at higher masses. Our results about the nucleus of FCC 277 are consistent with this picture. Certainly, a larger sample is needed to study in more detail whether gas dissipation is a common mechanism for NSCs growth in early-type galaxies, as it is in late-type ones (e.g. Walcher et al. 2006; Hartmann et al. 2011). The NSC accounts for ∼0.2 per cent of the total mass of FCC 277, thus it is not an outlier of the typical scaling relations in early-type galaxies (e.g. Ferrarese et al. 2006).

8 CONCLUDING REMARKS

In this paper, we present a pilot study of the detailed properties of NSCs in early-type galaxies. Although the nucleation frequency in galaxies is estimated to be ∼80 per cent, detailed data about the chemical and dynamical properties of NSCs exist mainly for spiral hosts. In early-type galaxies, this task observationally is not trivial due to the intrinsic brightness of the underlying galaxy light, as well as small angular extent of the NSCs, which at the distance of Fornax, span ∼0.1 arcsec in diameter. We showed that using current technology, it is indeed possible and valuable information about the formation mechanisms of NSCs can be obtained. As a pilot test case we chose the galaxy FCC 277, a nucleated early-type galaxy that belongs to the Fornax cluster. This is the only member of this galaxy cluster that has a conveniently located bright star that one can use as a natural guide star for the AO system.

Using SINFONI AO assisted observations, we observed the central 3 arcsec ×3 arcsec of the galaxy. Thus, we obtained maps of the stellar kinematics with *HST*-like spatial resolution of 0.165 arcsec (FWHM). Our velocity map (Fig. 5) shows clear rotation with a maximum at ∼0.6 arcsec from the galaxy centre, which overlaps with a maximum in the discyness of the fitted isophots on the galaxy image (Fig. 3). The NSC itself has an effective radius of 0.08 arcsec and does not rotate within our detection limit of ∼6 kms^{-1}. However, we observe a pronounced drop in the velocity dispersion in the central 1 arcsec that suggests the existence of a dynamically cold rotating sub-structure. Our dynamical modelling reveals that the nucleus of this galaxy is complex: corotation and counter-rotating, as well as non-rotating, stellar orbits are needed simultaneously to reproduce the observed kinematics (Fig. 9). The NSC seems to be embedded in a disc that is most likely younger and more metal rich than the main body of the galaxy (Fig. 11). Due to insufficient S/N we can only provide a conservative upper limit for a possible black hole of 10^7 $M_\odot$. All these facts point to a complex formation history of the nuclear region in FCC 277. Most likely gas dissipation and merging played an important role in shaping the nucleus of this galaxy. To check whether this is a common phenomenon among early-type galaxies, a larger sample is needed and can be obtained with current observing facilities.

ACKNOWLEDGEMENTS

We are grateful to the ESO astronomers who obtained the data presented in this paper in service mode operations at La Silla Paranal

Observatory. We acknowledge fruitful discussions with Eric Peng, David R. Silva, Jakob Walcher, Hans-Walter Rix, Jesus Falcón-Barroso. We thank Alister Graham, Max Spolaor and Mina Koleva for providing us with their results in tabular form. ML would like to thank the staff at the Astronomical Observatory of the University of Sofia for their hospitality, where parts of this research have been carried out. LI and AJ acknowledge Fondecyt, Fondap and Basal funding for this project. AJ is supported by the Chilean Ministry for the Economy, Development and Tourism's Programa Iniciativa Científica Milenio through grant P07-021-F, awarded to The Milky Way Millennium Nucleus, by Anillo ACT-086 and BASAL CATA PFB-06. We finally thank the referee for her/his valuable comments. This paper is dedicated to Mariika B. Ilieva (1926–2012) with a warm thank you for all the support.

REFERENCES

Barth A. J., Strigari L. E., Bentz M. C., Greene J. E., Ho L. C., 2009, ApJ, 690, 1031
Bekki K., Couch W. J., Shioya Y., 2006, ApJ, 642, L133
Binggeli B., Barazza F., Jerjen H., 2000, A&A, 359, 447
Blakeslee J. P., Jordán A., Mei S. et al., 2009, ApJ, 694, 556
Böker T., Laine S., van der Marel R. P., Sarzi M., Rix H.-W., Ho L. C., Shields J. C., 2002, AJ, 123, 1389
Bonnet H. et al., 2004, The ESO Messenger, 117, 17
Bruzual G., Charlot S., 2003, MNRAS, 344, 1000
Cappellari M., 2002, MNRAS, 333, 400
Cappellari M., 2008, MNRAS, 390, 71
Cappellari M., Copin Y., 2003, MNRAS, 342, 345
Cappellari M., Emsellem E., 2004, PASP, 116, 138
Cappellari M. et al., 2006, MNRAS, 366, 1126
Cappellari M. et al., 2007, MNRAS, 379, 418
Capuzzo-Dolcetta R., Miocchi P., 2008a, ApJ, 681, 1136
Capuzzo-Dolcetta R., Miocchi P., 2008b, MNRAS, 388, L69
Carollo C. M., Stiavelli M., Mack J., 1998, AJ, 116, 68
Côté P. et al., 2006, ApJS, 165, 57
Côté P. et al., 2007, ApJ, 671, 1456
Davies R., Agudo Berbel A., Wiezorrek E., Ott T., Förster Schreiber N. M., 2010, in McClean I., Ramsay S., Takami H., eds, Proc. SPIE Conf. Ser. Vol. 7735, Ground-based and Airborne Instrumentation for Astronomy III. SPIE, Bellingham, p. 77356V
Eisenhauer F. et al., 2003, in Iye M., Moorwood A. F. M., eds, Proc. SPIE Conf. Ser. Vol. 4841, SINFONI – Integral Field Spectroscopy at 50 Milli-arcsecond Resolution with the ESO VLT. SPIE, Bellingham, p. 1548
Emsellem E. et al., 2007, MNRAS, 379, 401
Emsellem E. et al., 2011, MNRAS, 414, 888
Ferguson H. C., 1989, AJ, 98, 367
Ferrarese L. et al., 2006, ApJ, 644, L21
Frogel J. A., Stephens A., Ramírez S., DePoy D. L., 2001, AJ, 122, 1896
Graham A. W., Colless M. M., Busarello G., Zaggia S., Longo G., 1998, A&AS, 133, 325
Graham A. W., Spitler L. R., 2009, MNRAS, 397, 2148
Hartmann M., Debattista V. P., Seth A., Cappellari M., Quinn T. R., 2011, MNRAS, 418, 2697
Jordán A. et al., 2007, ApJS, 169, 213
Koleva M., Prugniel P., de Rijcke S., Zeilinger W. W., 2011, MNRAS, 417, 1643
Krajnović D., Cappellari M., de Zeeuw P. T., Copin Y., 2006, MNRAS, 366, 787
Krist J., 1995, in Shaw R. A., Payne H. E., Hayes J. J. E., eds, ASP Conf. Ser. Vol. 77, Simulation of HST PSFs using Tiny Tim. Astron. Soc. Pac., San Francisco, p. 349
Lyubenova M., Kuntschner H., Rejkuba M., Silva D. R., Kissler-Patig M., Tacconi-Garman L. E., Larsen S. S., 2010, A&A, 510, A19
Maraston C., 2005, MNRAS, 362, 799
Mármol-Queraltó E., Cardiel N., Cenarro A. J., Vazdekis A., Gorgas J., Pedraz S., Peletier R. F., Sánchez-Blázquez P., 2008, A&A, 489, 885
Mármol-Queraltó E. et al., 2009, ApJ, 705, L199
Mihos J. C., Hernquist L., 1994, ApJ, 437, L47
Neumayer N., Walcher C. J., 2012, Adv. Astron., 2012
Neumayer N., Walcher C. J., Andersen D., Sánchez S. F., Böker T., Rix H.-W., 2011, MNRAS, 413, 1875
Oh K. S., Lin D. N. C., 2000, ApJ, 543, 620
Padilla N. D., Strauss M. A., 2008, MNRAS, 388, 1321
Peletier R. F., Davies R. L., Illingworth G. D., Davis L. E., Cawson M., 1990, AJ, 100, 1091
Peng E. W. et al., 2006, ApJ, 639, 95
Pflamm-Altenburg J., Kroupa P., 2009, MNRAS, 397, 488
Piqueras López J., Davies R., Colina L., Orban de Xivry G., 2012, ApJ, 752, 47
Rossa J., van der Marel R. P., Böker T., Gerssen J., Ho L. C., Rix H.-W., Shields J. C., Walcher C.-J., 2006, AJ, 132, 1074
Rousselot P., Lidman C., Cuby J.-G., Moreels G., Monnet G., 2000, A&A, 354, 1134
Schwarzschild M., 1979, ApJ, 232, 236
Seth A. C., Blum R. D., Bastian N., Caldwell N., Debattista V. P., 2008, ApJ, 687, 997
Seth A. C., Dalcanton J. J., Hodge P. W., Debattista V. P., 2006, AJ, 132, 2539
Seth A. C. et al., 2010, ApJ, 714, 713
Silva D. R., Kuntschner H., Lyubenova M., 2008, ApJ, 674, 194
Spolaor M., Hau G. K. T., Forbes D. A., Couch W. J., 2010, MNRAS, 408, 254
Tremaine S. D., Ostriker J. P., Spitzer L. Jr, 1975, ApJ, 196, 407
Turner M. L., Cote P., Ferrarese L., Jordan A., Blakeslee J. P., Mei S., Peng E. W., West M. J., 2012, ApJS, 203, 5
van de Ven G., de Zeeuw P. T., van den Bosch R. C. E., 2008, MNRAS, 385, 614
van den Bosch R. C. E., de Zeeuw P. T., 2010, MNRAS, 401, 1770
van den Bosch R. C. E., van de Ven G., Verolme E. K., Cappellari M., de Zeeuw P. T., 2008, MNRAS, 385, 647
Walcher C. J. et al., 2005, ApJ, 618, 237
Walcher C. J., Böker T., Charlot S., Ho L. C., Rix H.-W., Rossa J., Shields J. C., van der Marel R. P., 2006, ApJ, 649, 692
Wegner G. et al., 2003, AJ, 126, 2268
Wehner E. H., Harris W. E., 2006, ApJ, 644, L17

This paper has been typeset from a TEX/LATEX file prepared by the author.